

## Effect of the Li Reduction to Electrodeposition of Nd-Sn Compounds in Liquid Sn Electrode in LiCl-KCl-NdCl<sub>3</sub> Melt

Sun, Chenteng; Xu, Qian; Yang, Yongxiang; Zou, Xingli; Cheng, Hongwei; Lu, Xionggang

**DOI**

[10.1149/1945-7111/ac2fc7](https://doi.org/10.1149/1945-7111/ac2fc7)

**Publication date**

2021

**Document Version**

Final published version

**Published in**

Journal of the Electrochemical Society

**Citation (APA)**

Sun, C., Xu, Q., Yang, Y., Zou, X., Cheng, H., & Lu, X. (2021). Effect of the Li Reduction to Electrodeposition of Nd-Sn Compounds in Liquid Sn Electrode in LiCl-KCl-NdCl<sub>3</sub> Melt. *Journal of the Electrochemical Society*, 168(10), Article 102505. <https://doi.org/10.1149/1945-7111/ac2fc7>

**Important note**

To cite this publication, please use the final published version (if applicable). Please check the document version above.

**Copyright**

Other than for strictly personal use, it is not permitted to download, forward or distribute the text or part of it, without the consent of the author(s) and/or copyright holder(s), unless the work is under an open content license such as Creative Commons.

**Takedown policy**

Please contact us and provide details if you believe this document breaches copyrights. We will remove access to the work immediately and investigate your claim.

## Effect of the Li Reduction to Electrodeposition of Nd-Sn Compounds in Liquid Sn Electrode in LiCl-KCl-NdCl<sub>3</sub> Melt

To cite this article: Chenteng Sun *et al* 2021 *J. Electrochem. Soc.* **168** 102505

View the [article online](#) for updates and enhancements.



The Electrochemical Society  
Advancing solid state & electrochemical science & technology

### 241st ECS Meeting

May 29 – June 2, 2022 Vancouver • BC • Canada

Abstract submission deadline: Dec 3, 2021

Connect. Engage. Champion. Empower. Accelerate.  
**We move science forward**



**Submit your abstract**





# Effect of the Li Reduction to Electrodeposition of Nd-Sn Compounds in Liquid Sn Electrode in LiCl-KCl-NdCl<sub>3</sub> Melt

Chenteng Sun,<sup>1</sup> Qian Xu,<sup>1,z</sup> Yongxiang Yang,<sup>2,3</sup> Xingli Zou,<sup>1</sup> Hongwei Cheng,<sup>1</sup> and Xionggang Lu<sup>1</sup>

<sup>1</sup>State Key Laboratory of Advanced Special Steel & Shanghai Key Laboratory of Advanced Ferrometallurgy & School of Materials Science and Engineering, Shanghai University, Shanghai 200072, People's Republic of China

<sup>2</sup>Department of Materials Science and Engineering, Delft University of Technology, 2628 CD Delft, The Netherlands

<sup>3</sup>Department of Metallurgical Engineering, Anhui University of Technology, Ma'anshan 243002, People's Republic of China

The electrochemical behaviors of Li<sup>+</sup> and Nd<sup>3+</sup> were investigated on W, liquid Sn pool and Sn film electrodes in LiCl-KCl-NdCl<sub>3</sub> melt at 673 K. Various electrochemical techniques, such as cyclic voltammogram, square wave voltammogram, and open circuit chronopotentiometry, were conducted to evaluate the electrochemical behaviors of Li<sup>+</sup> and Nd<sup>3+</sup>. The reduction of Nd<sup>3+</sup> was found to be a two-step process in the W electrode and a one-step process in the liquid Sn electrode. During the formation of the Nd-Sn intermetallic compounds, only the NdSn<sub>3</sub> would be formed without the reduction of the Li<sup>+</sup> in the liquid Sn electrode. When the reduction potential moves over -2.77 V vs Cl<sub>2</sub>/Cl<sup>-</sup>, the Li<sup>+</sup> in the electrolyte would inevitably be reduced into the liquid Sn electrode. The Nd-Sn intermetallic compounds were deposited on the liquid Sn pool electrode at -2.74 V vs Cl<sub>2</sub>/Cl<sup>-</sup> in the LiCl-KCl-NdCl<sub>3</sub> melts for 5 h. The products were characterized by SEM-EDS and XRD. The loose product on the surface of the deposition displayed the existence of NdSn<sub>3</sub> in Nd-Sn intermetallic compounds. The high content of Nd inclusion formed by segregation was detected in the solidified Sn electrode.

© 2021 The Electrochemical Society ("ECS"). Published on behalf of ECS by IOP Publishing Limited. [DOI: 10.1149/1945-7111/ac2fc7]

Manuscript submitted August 27, 2021; revised manuscript received September 28, 2021. Published October 27, 2021.

Supplementary material for this article is available [online](#)

Neodymium is a representative rare earth element, which is widely used as an additive to improve the alloys' properties, such as Mg alloys<sup>1-3</sup> and Zn alloys.<sup>4,5</sup> Considering the segregation during preparation of Nd alloys by adding metallic Nd into molten alloys, researchers tried to use molten salt electrolysis to prepare Nd alloys. Electrodeposition with liquid cathode is a promising way to prepare alloys with low cell voltage and operation temperature, which decreases the energy consumption and improves the current efficiency.<sup>6</sup> Therefore, many researchers investigated the reduction of the Nd<sup>3+</sup> in the different liquid metallic electrodes. Luo et al.<sup>7</sup> used the liquid Zn as the cathode and investigated the electrochemical behaviors of Nd<sup>3+</sup> in the Zn electrode. De Córdoba, G. et al.<sup>8</sup> investigated the activity coefficient of Nd in the liquid Al. Smolenski, V. et al.<sup>9</sup> obtained the thermodynamics data of Nd<sup>3+</sup> in the gallium-indium alloy. Besides, liquid Ga,<sup>10</sup> Bi<sup>11</sup> electrodes were also applied to measure the electrochemical behaviors of Nd.

In these works,<sup>7,9-12</sup> LiCl-KCl eutectic was usually chosen as electrolyte because of its low melting point. However, during the reduction process of Nd<sup>3+</sup>, the Li<sup>+</sup> in the electrolyte would also be reduced and dissolved in the liquid electrodes, especially in liquid Sn electrode. The consumption of Li would decrease the content of LiCl in the electrolyte, which would increase the melting point of the electrolyte. Besides, the reduced Li in the Sn electrode would also affect the purity of the product. However, few works are focus on the effect of the reduction of Li<sup>+</sup> on liquid Sn electrode during the preparation of Nd-Sn alloys.

In this work, the electrochemical behaviors of Li<sup>+</sup> and Nd<sup>3+</sup> in LiCl-KCl-NdCl<sub>3</sub> on the liquid Sn electrode were investigated. Various electrochemical technologies, such as cyclic voltammogram (CV), square wave voltammogram (SWV), open circuit chronopotentiometry (OCP) and chronoamperometry (CA) were implemented to evaluate the electrochemical behaviors of Li<sup>+</sup> and Nd<sup>3+</sup>. Through the measurement, the reduction potential of Li<sup>+</sup> in the liquid Sn electrode was obtained and the reduction potential range for Nd<sup>3+</sup> and the Nd-Sn alloys were also determined.

## Experimental

**Chemical.**—In this work, lithium and potassium chloride (anhydrous, AR grade, Sinopharm Chemical Reagent Co., Ltd.) and neodymium chloride (anhydrous, 99.9%, Aladdin) were used for the studies. The mixture electrolyte (LiCl:KCl = 45: 55 wt.%) was weighted and pre-dried in a muffle furnace at 573 K for more than 72 h to remove the moisture. Then the mixture in the alumina crucible (99%, Shanghai Gongtao Ceramics Co., Ltd.) moved to sealed stainless steel reactor cell in the electric furnace. The electrolyte was handled under the argon atmosphere. The schematic of electrolytic cell is shown in Fig. 1a. The cell was heated to the 673 K and stayed for 5 h to keep the temperature stabilizes. Then, the NdCl<sub>3</sub> was directly introduced into the melt. The electrochemical measurements were conducted after 5 h to dissolve the NdCl<sub>3</sub> into the electrolyte.

**Electrodes and instrumentation.**—In the experiments, three-electrodes cell was assembled for the electrochemical measurements. Graphite rods were served as the counter electrodes. The AgCl/Ag electrode was applied as the reference electrode. It consisted of a silver wire 0.2 mm with inserted into a closed-end alumina tube (99%, Shanghai Gongtao Ceramics Co., Ltd.), containing LiCl-KCl-1 mol% AgCl. The bottom of the closed-end alumina tube was sanded to conduct ionic. According to the Ref. 13, the AgCl/Ag electrode potential was -1.13 V vs Cl<sub>2</sub>/Cl<sup>-</sup> at 673 K in LiCl-KCl eutectic. So, all potentials in this work were transferred to the potentials referred to the Cl<sub>2</sub>/Cl<sup>-</sup>. In the experiments, three kinds of electrodes were used as the working electrodes, which are tungsten (W) electrode, Sn film electrode and liquid Sn pool electrode, respectively. Three working electrodes were present in Fig. 1b. The Sn film electrode shown in Fig. 1c was made of a W wire taking from molten Sn pool. The Sn adhere on the surface of the W wire was solidified and formed a thin Sn film. By measuring the diameter of W wire the before and after coating Sn film, the thickness of Sn film was determined to be 0.14 mm. The liquid tin pool electrode was made of a molybdenum (Mo) wire connected with the tin block, as shown in Fig. 1d. The Mo wire was protected with the quartz tube to isolate the electrolyte. The difference between liquid Sn pool electrode and Sn film electrode was their amount of Sn in the electrode.

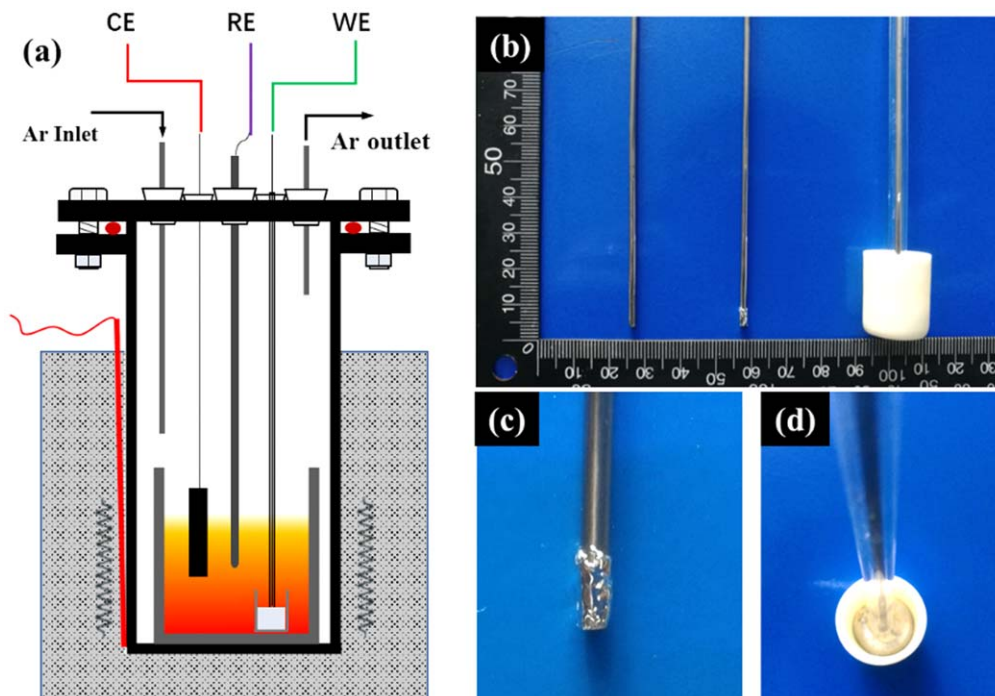


**Figure 1.** (a) Schematic of electrolytic cell and photo of (b) working electrode including (c) Sn film electrode and (d) liquid Sn pool electrode.

**Instrumentation.**—In the experiments, electrochemical measurements like CV, SWV, OCP and CP were conducted by PARSTAT 4000 A (Princeton Applied Research) potentiostat/galvanostat controlled with the Versa Studio software.

The electrochemical deposition of Nd-Sn intermetallic compound was carried out on liquid tin electrode in LiCl-KCl-NdCl<sub>3</sub> melts. The deposition products were washed by deionized water and ethanol with ultrasound to remove the solidified melt.

The X-ray diffraction (XRD, a Bruker-AXS D8 Advance) was applied to explore the crystalline structure of the reduced products. The deposition was characterized using Scanning Electron Microscopy (SEM, FEI Nova Nano 450) equipped with energy dispersive X-ray detector (EDX, Oxford INCA EDS system) to obtain their surface morphology and micro composition.

## Result and Discussion

**Electrochemical behaviors of Li<sup>+</sup> and Nd<sup>3+</sup>.**—Figure 2a presents the CV curves of LiCl-KCl before and after adding NdCl<sub>3</sub> on the W at 673 K, respectively. In the LiCl-KCl melt, except the cathodic

current limit R1 and corresponding oxidization peak O1, which were related to the reduction/oxidation of metallic Li, no other redox peaks were found in the CV curve. It indicated that no impurities exist in the LiCl-KCl melt. After the addition of NdCl<sub>3</sub>, two pair of redox peaks R2/O2 and R3/O3 appeared in the CV curve. According to the Ref. 7, 14, they should correspond to the deposition/dissolution of metallic Nd. The reduction peaks R2, R3 and oxidization peak O3 in the CV curve were unobvious and hard to be detected. Therefore, a sensitive electrochemical technology, SWV, was applied to evaluate the reduction behaviors of Nd<sup>3+</sup>. Figure 2b represents the SWV curves of LiCl-KCl-NdCl<sub>3</sub> on the W electrode at 673 K.

In the Fig. 2b, two obvious cathodic peaks, R2 and R3, were found at -3.3 and -3.5 V in the SWV curve. The existence of cathodic peak R3 is the evidence of the anodic peak O3. Based on the relationship between the width of half peak ( $W_{1/2}$ ) and the number of transferred electrons ( $n$ ) in Eq. 1, the number of transferred electrons for reduction peaks R2 and R3 with different frequencies could be calculated and results are presented in Table I.

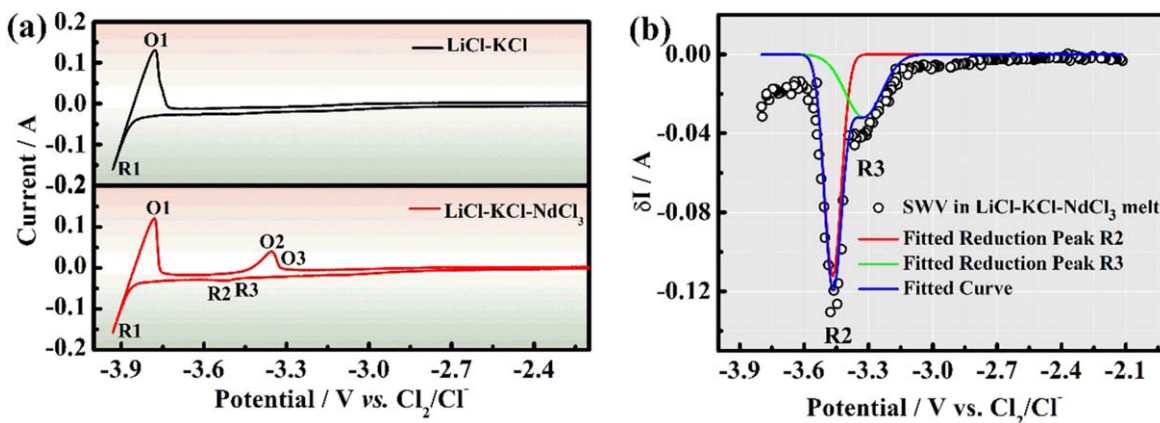


**Figure 2.** (a) CVs for W electrode in LiCl-KCl and LiCl-KCl- $9.6 \times 10^{-5}$  mol·cm<sup>-3</sup> NdCl<sub>3</sub> at 673 K, scan rate: 0.1 V s<sup>-1</sup>. (b) SWV for W electrode in LiCl-KCl- $9.6 \times 10^{-5}$  mol·cm<sup>-3</sup> NdCl<sub>3</sub> at 673 K, Frequency: 20 Hz.

**Table I. The width of half peak and number of transferred electrons with different frequency in SWV curves on the W and liquid tin electrode at 673 K.**

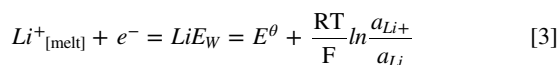
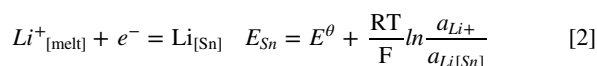
f/Hz	R2			R3		
	$W_{1/2}$	$n$	$n_{ave}$	$W_{1/2}$	$n$	$n_{ave}$
10	0.081	2.53		0.203	1.01	
20	0.098	2.09	2.31	0.141	1.44	1.13
30	0.088	2.31		0.216	0.94	

$$W_{1/2} = 3.52RT/nF \quad [1]$$

where R is the ideal gas constant,  $8.314 \text{ J}\cdot\text{mol}^{-1}\cdot\text{K}^{-1}$ ; T is the Kelvin temperature, K; F is the Faraday constant,  $96485 \text{ C}\cdot\text{mol}^{-1}$ .

Through the calculation, the average number of transferred electrons for the reduction peak R2 and R3 are 2.31 and 1.13, respectively. It indicates that the reduction of  $\text{Nd}^{3+}$  on the W electrode is a two-step reduction process. The intermediate valence compound,  $\text{Nd}^{2+}$ , would be formed during the reduction process. The results are accorded with the previous research.<sup>12</sup>

**Electrochemical behaviors of  $\text{Li}_{[\text{Sn}]}$  and  $\text{Nd}_{[\text{Sn}]}$ .**—When the liquid Sn pool electrode was applied to measure the electrochemical behaviors of Li and Nd, they were quite different from those on W electrode. The black curve in Fig. 3a represents the CV curves of LiCl-KCl melts on the liquid Sn pool electrode. According to the literatures,<sup>15,16</sup> the anodic limit O5 and corresponding reduction peak R5 were caused by the anodic dissolution and cathodic deposition of the liquid tin electrode. The cathodic current limit R4 was attributed to the deposition of Li dissolved in the liquid Sn pool electrode ( $\text{Li}_{[\text{Sn}]}$ ). The reduction reactions of  $\text{Li}^+$  on the liquid Sn pool and W electrode and their corresponding reduction potentials were shown in Eqs. 2–3.



where  $E_{\text{Sn}}$  and  $E_W$  are the reduction potentials of  $\text{Li}^+$  in liquid Sn pool and W electrodes, respectively;  $E^\theta$  is the standard potential of the reduction reaction of  $\text{Li}^+$ ,  $a_{\text{Li}^+}$ ,  $a_{\text{Li}_{[\text{Sn}]}}$  and  $a_{\text{Li}}$  are the activities of Li ions, Li dissolved in the liquid Sn pool and metallic Li, respectively; R, T, F represent the same meanings in Eq. 1.

Compared with cathodic current limit R1 on the W electrode in Fig. 2a, the cathodic potential of R4 on the liquid Sn pool electrode was obviously shift to the positive direction, which is called “depolarization effect.” It is caused by the activities difference between metallic Li and  $\text{Li}_{[\text{Sn}]}$ . The activity of  $\text{Li}_{[\text{Sn}]}$  is lower than metallic Li on the W electrode. According to the Nernst equation in Eqs. 2–3, the  $\text{Li}^+$  reduction potential difference between liquid Sn pool electrode and W electrode, as shown in Eq. 4, is greater than zero. That explained the positive shift of reduction potential of  $\text{Li}_{[\text{Sn}]}$ . Similar results were also reported on the references.<sup>17–19</sup> From the CV curve, the onset potential of R4 is  $-2.75 \text{ V}$  vs  $\text{Cl}_2/\text{Cl}^-$ .

$$\Delta E = E_{\text{Sn}} - E_W = \frac{RT}{F} \ln \frac{a_{\text{Li}}}{a_{\text{Li}_{[\text{Sn}]}}} \quad [4]$$

The red curve in Fig. 3a represents the CV curves of LiCl-KCl-NdCl<sub>3</sub> melts on the liquid Sn pool electrode. Except the redox peaks R6/O6 are observed at the CV curve, which is associated with the deposition/dissolution of the Nd dissolved in the liquid Sn electrode ( $\text{Nd}_{[\text{Sn}]}$ ). Due to the depolarization effect, the redox potential of Nd on liquid Sn pool electrode also shift to the positive direction. The onset potential of R6 is observed at  $-2.5 \text{ V}$  vs  $\text{Cl}_2/\text{Cl}^-$ . The reduction potential difference between Nd and Li in liquid Sn pool electrode is smaller than those in the W electrode, which means that the potential range to selectively separate Li and Nd in the liquid Sn electrode is narrower than that in the W electrode.

It is worth to notice that, during the reduction of  $\text{Nd}^{3+}$  in the Sn pool electrode, only one reduction peak R6 is found in the CV curve, which is different with the result in Fig. 2. Therefore, SWV was applied to evaluate the reduction process of Nd in liquid Sn pool electrode. Figure 3b shows the SWV curves of LiCl-KCl and LiCl-KCl-NdCl<sub>3</sub> melts on the liquid Sn pool electrode at 673 K. In LiCl-KCl melt, only the current limit R4 started at  $-1.8 \text{ V}$  appears in the SWV curve, which is related to the reduction of Li in the liquid Sn pool electrode. After the addition of NdCl<sub>3</sub>, except the reduction current limit R4, only one reduction peak R6 appears in the SWV curve. According to the result from CV curve, the reduction peak R6 is caused by the deposition of Nd dissolved in the liquid Sn pool electrode. Unlike the two-step reduction process of  $\text{Nd}^{3+}$  on W electrode, the reduction of  $\text{Nd}^{3+}$  turn into one-step reduction process on the liquid Sn pool electrode. Similar result was also reported by other literatures.<sup>6,20,21</sup> According to the reduction peak potential of R3 and R6, the reduction potential of  $\text{Nd}_{[\text{Sn}]}$  on the liquid Sn pool electrode is more positive than that of the formation of  $\text{Nd}^{2+}$  on the W electrode in the melt. Therefore, the Gibbs formation energy of  $\text{Nd}_{[\text{Sn}]}$  in the liquid Sn pool is lower than that of  $\text{Nd}^{2+}$  in the melt, which indicates the  $\text{Nd}^{3+}$  in the melt prefer to form  $\text{Nd}_{[\text{Sn}]}$  in the Sn pool rather than  $\text{Nd}^{2+}$  in the melt. That explains the different

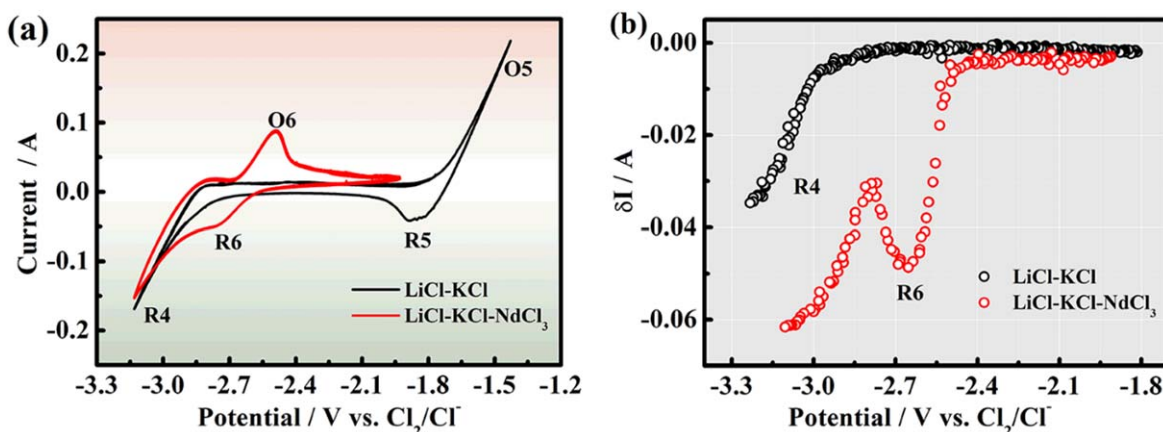


**Figure 3.** (a) CVs and (b) SWVs for Sn pool electrode in LiCl-KCl and LiCl-KCl- $9.6 \times 10^{-5} \text{ mol}\cdot\text{cm}^{-3} \text{ NdCl}_3$  at 673 K, scan rate: 0.1 V/s, Frequency: 20 Hz.

reduction processes in W and liquid Sn pool electrodes. The one-step reduction process of  $\text{Nd}^{3+}$  would limit the disproportionation reaction of  $\text{Nd}^{3+}$ , which is helpful to reduce the energy consumption and increase the current efficiency.

**Electrochemical behaviors of Li-Sn and Nd-Sn intermetallic compounds.**—In the liquid Sn pool electrode, the reduced Li and Nd during the measurement were totally dissolved inside and no Li-Sn or Nd-Sn intermetallic compounds would be formed. However, in the liquid Sn film electrode, due to the limited amount of Sn, the reduced Li and Nd in the Sn film electrode would quickly exceed their saturate solubilities and formed Li-Sn and Nd-Sn intermetallic compounds. In order to obtain electrochemical behaviours of Nd-Sn and Li-Sn intermetallic compounds, Sn film electrode was applied to the measurement.

Figure 4a shows the CV curves of liquid Sn film electrode in LiCl-KCl melt with different potential range at 673 K. According to the previous work, the redox peaks (R1/O1, R4/O4) were related to the reduction/oxidization peaks of metallic Li and the  $\text{Li}_{[\text{Sn}]}$ . Except them, there are six oxidation peaks and four reduction peaks observed in the CV curves, which are related to the dissolution/formation of Sn-Li intermetallic compounds. The reduction peaks R9 and R10 were confirmed by their corresponding oxidation peaks at different scan range. Except R1/O1 and R4/O4, there were six redox peaks (R7/O7 ~ R12/O12) found in the CV curve, which meant the six Li-Sn intermetallic compounds were formed during the measurements. It is accorded with the number of Li-Sn intermetallic compounds in the Li-Sn binary phase diagram at 673 K.<sup>22</sup> According to the Li-Sn phase diagram (shown in Fig. S1 available online at [stacks.iop.org/JES/168/102505/mmedia](https://stacks.iop.org/JES/168/102505/mmedia)), the intermetallic compounds in CV curves in Fig. 4a from R12/O12 to R7/O7 were  $\text{LiSn}$ ,  $\text{Li}_7\text{Sn}_3$ ,  $\text{Li}_5\text{Sn}_3$ ,  $\text{Li}_7\text{Sn}_2$ ,  $\text{Li}_{13}\text{Sn}_5$  and  $\text{Li}_{22}\text{Sn}_5$  in sequence.

Considering the reduction potential of metallic Nd on the W electrode is  $-3.5$  V, the formation potentials of Nd-Sn intermetallic compounds should stay between  $-3.5$  V and  $-2.5$  V. Figure 4b shows the CV curves of liquid Sn film electrode in LiCl-KCl-NdCl<sub>3</sub> melt at 673 K. According to the CV curve in Fig. 4a, the redox peaks (R11/O11, R12/O12) were correspond to Li-Sn intermetallic compounds and redox peaks R4/O4 were related to the redox of  $\text{Li}_{[\text{Sn}]}$ . Except them, another two pairs of redox peaks R13/O13 and R14/O14 were observed around  $-3.1/-2.9$  and  $-2.7/-2.6$  V, which should be ascribed to the reduction/oxidization of Nd-Sn intermetallic compounds. It is interesting to see that although there are nine Nd-Sn intermetallic compounds in Nd-Sn binary phase diagram<sup>23</sup> (shown in the Fig. S2), only two kinds of Nd-Sn intermetallic compounds were observed in the CV curve in Fig. 4b.

To further detect the equilibrium potential of Nd-Sn intermetallic compounds, OCP was also conducted to evaluate the Li-Sn and Nd-Sn intermetallic compounds. Figure 5a shows the OCP curve after

electrodepositing at  $-50$  mA for 50 s in LiCl-KCl melt. The curve I in Fig. 5a was the OCP curve obtained on the W electrode. The potential plateau 1 presents the oxidization process of metallic Li. The curve II in Fig. 5a shows the OCP curve measured on the Sn film electrode. With the application of Sn film electrode, various potential plateaus appeared in the Curve II, which are considered to be the oxidization of different Li-Sn intermetallic compounds. According to the Li-Sn phase diagram, the Li-Sn intermetallic compounds in curve II from positive to negative are  $\text{LiSn}$ ,  $\text{Li}_7\text{Sn}_3$ ,  $\text{Li}_5\text{Sn}_3$ ,  $\text{Li}_{13}\text{Sn}_5$ ,  $\text{Li}_7\text{Sn}_2$ ,  $\text{Li}_{22}\text{Sn}_5$  and Li, respectively. The unobvious potential plateaus 4, 5 are accorded with the oxidization peaks O9 and O10 in the CV curve in Fig. 4b. Compared with the other Li-Sn intermetallic compounds' potential plateaus, the short duration time of plateaus 4, 5 are caused by the low number of transferred electrons of the oxidization process of  $\text{Li}_5\text{Sn}_3$ ,  $\text{Li}_{13}\text{Sn}_5$ . According to the OCP curve, the equilibrium potential of intermetallic compound  $\text{LiSn}$  is  $-3.27$  V, which is more negative than that of  $\text{Li}_{[\text{Sn}]}$ .

Figure 5b shows the OCP curves all measured after electrodepositing at  $-3.63$  V for 20 s. The curve III presents the OCP curve obtained in LiCl-KCl-NdCl<sub>3</sub> melt on W electrode. The plateau 8 at  $-3.5$  V represented the oxidization of metallic Nd on W electrode. The curve IV and curve V shows the OCP curves obtained on Sn film electrode in LiCl-KCl and LiCl-KCl-NdCl<sub>3</sub> melts, respectively. The plateaus in OCP curve IV are accorded with the Li-Sn intermetallic compounds. After the addition of NdCl<sub>3</sub>, the plateau 3 was missing and plateau 9 appeared in curve V. The absence of plateau 3 should attribute to the limited deposit time, which could not further form  $\text{Li}_7\text{Sn}_2$ . The new appeared plateau 9 at  $-2.6$  V indicated the formation of Nd-Sn intermetallic compounds during the reduction process. The plateau 9 is accord with oxidization peak O14 in the CV curve in Fig. 4b.

According to the previous work, to limited the formation of Li-Sn intermetallic compounds, the OCP curve on Sn film electrode measured after  $-3.13$  V for 1000 s in LiCl-KCl-NdCl<sub>3</sub>, which is shown as curve VI in Fig. 5c. Except plateau 9 mentioned in curve V, two unobvious plateaus (10 and 11) appeared at  $-2.77$  and  $-2.9$  V. According to the CV curves, the plateau 10 is related to oxidization of  $\text{Li}_{[\text{Sn}]}$  and the plateaus 11 corresponds to the dissolution of the Nd-Sn intermetallic compounds O13. According to the Nd-Sn phase diagram, plateau 11 represents the  $\text{Nd}_2\text{Sn}_5$ .

Combined with the result from the CV and OCP curves, it is clear to see that the reduction potential of  $\text{Li}_{[\text{Sn}]}$  stays between that of  $\text{NdSn}_3$  and  $\text{Nd}_2\text{Sn}_5$ . Therefore, during the reduction of Nd in the liquid Sn electrode, no Li would be reduced in the liquid Sn electrode during the formation of  $\text{NdSn}_3$  and  $\text{Nd}_{[\text{Sn}]}$ . However, due to the more negative reduction potential of  $\text{Nd}_2\text{Sn}_5$ , as shown in Fig. 5d, the Li would be reduced in the liquid Sn electrode during the formation of the  $\text{Nd}_2\text{Sn}_5$ , which means that the reduction of Li is inevitable during the preparation of  $\text{Nd}_2\text{Sn}_5$  and other high

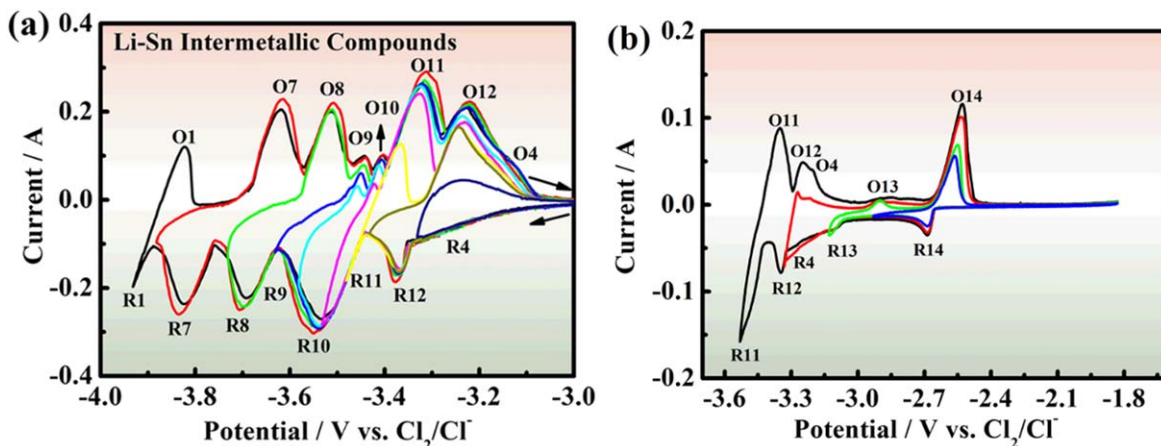
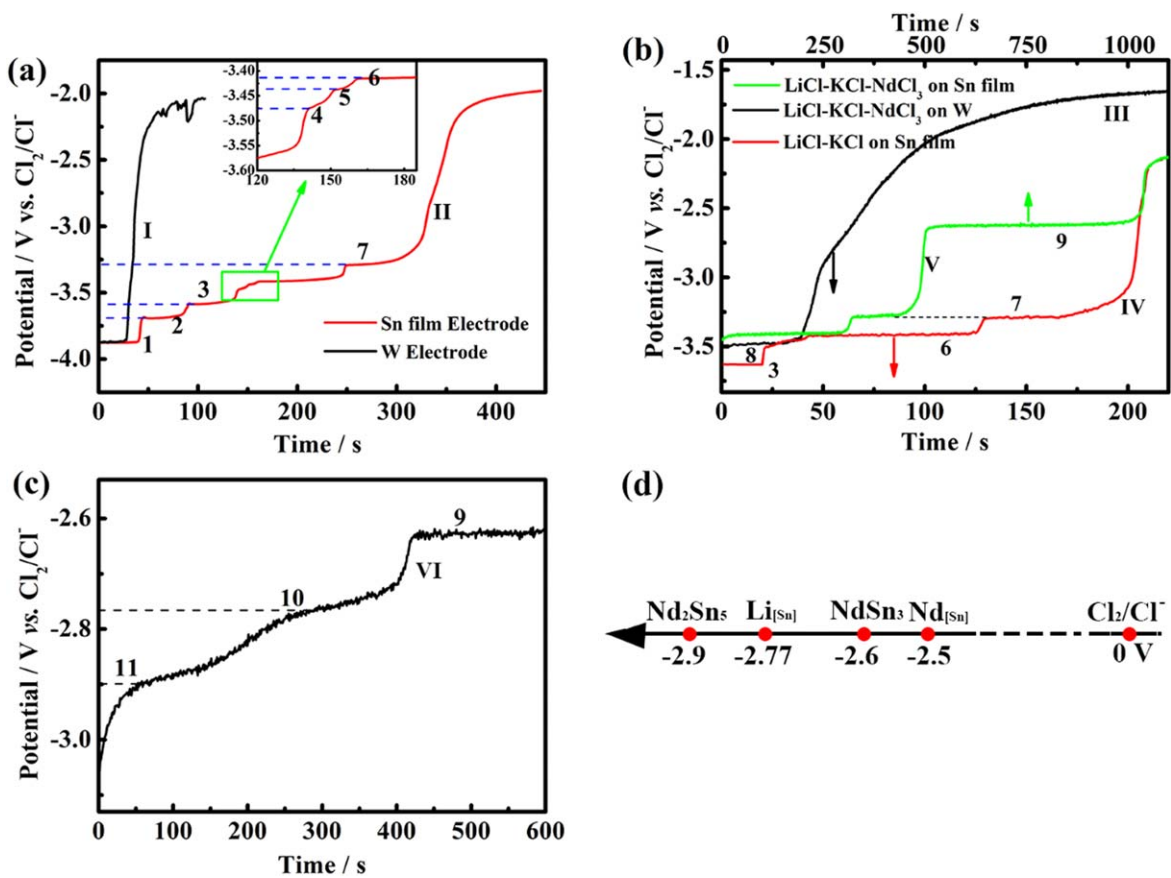


Figure 4. CVs for liquid Sn film electrode in (a) LiCl-KCl and (b) LiCl-KCl- $9.62 \times 10^{-5}$  mol·cm<sup>-3</sup> NdCl<sub>3</sub> at 673 K at different scan range, scan rate: 0.1 V s<sup>-1</sup>.



**Figure 5.** (a) OCP curves on W electrode (black line) and Sn film electrode (red line) after electrodepositing at  $-50$  mA for 50 s in LiCl-KCl melt; (b) OCP curves after electrodepositing at  $-3.63$  V for 20 s in LiCl-KCl on Sn film electrode (red line) and in LiCl-KCl- $9.62 \times 10^{-5}$  mol·cm<sup>-3</sup> NdCl<sub>3</sub> melts on W electrode (black line) and Sn film electrode (green line), (c) OCP curves on Sn film electrode (black line) after electrodepositing at  $-3.13$  V for 1000 s in LiCl-KCl- $9.62 \times 10^{-5}$  mol·cm<sup>-3</sup> NdCl<sub>3</sub> melt, (d) reduction potentials of Li and Nd in Sn electrode in LiCl-KCl- $9.62 \times 10^{-5}$  mol·cm<sup>-3</sup> NdCl<sub>3</sub> melt at 673 K.

Nd-contained Nd-Sn intermetallic compounds. The reduction of Li would limit the formation of Nd-Sn intermetallic compounds with high content of Nd. That explained why only two kinds of Nd-Sn intermetallic compounds were found during the measurement. Besides, the reduction of the Li would decrease current efficiency and purity of the product.

#### Preparation and characterization of the cathodic deposits.—

Based on the previous results,  $-2.74$  V is negative enough to reduce Nd in the liquid tin electrode without the reduction of Li in liquid Sn electrode. Therefore, potentiostatic electrolysis was implemented in the liquid Sn pool electrode at  $-2.74$  V for 5 h. The reduced product was washed by deionized water to remove the chloride salt. Figure 6 shows the chronoamperometry curve and the photo of reduced product. From the morphology of the deposition, it is obvious that the bottom product is solidified liquid tin electrode. The upper product is porous and should be Nd-Sn intermetallic compounds.

Figure 7a shows the XRD patterns of the upper product obtained at  $-2.74$  V for 5 h. According to the XRD pattern, Sn, NdSn<sub>3</sub> and NdOCl are detected in the precipitated phase. The NdOCl comes from two ways. The oxidation of NdCl<sub>3</sub> with O<sub>2</sub> might cause the formation of NdOCl. Besides, during preparing the sample,<sup>16</sup> the deionized water was used to remove the LiCl-KCl melt, which might also cause the hydrolysis of NdCl<sub>3</sub>. Therefore, the formation of NdOCl was based upon the interaction of all of these factors. The existent of NdSn<sub>3</sub> proved the R14 belonged to the NdSn<sub>3</sub>. The SEM image of the product in Figs. 7b–7c also shows the loose structure. The porous structure was caused by the formation of Nd-Sn intermetallic compounds. Similar phenomenon was also report on Li-Sn alloy.<sup>24</sup> The loose structure would be helpful to the diffusion

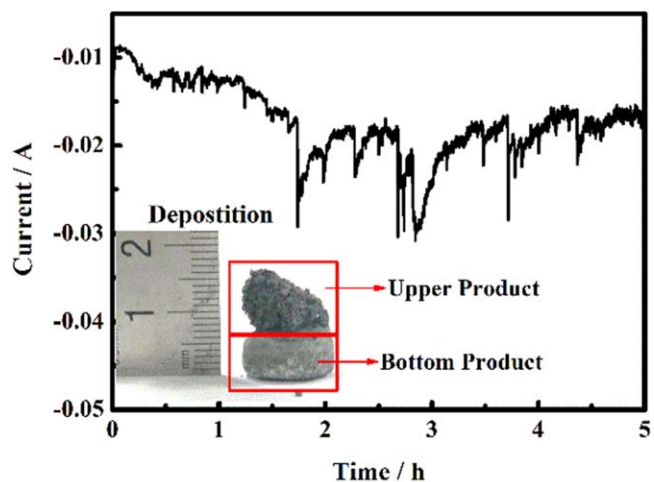


**Figure 6.** Chronoamperometry curve at  $-2.74$  V for 5 h and the digital photo of the product.

of the Nd<sup>3+</sup> moving to the surface of the liquid Sn electrode during the reduction process. According to the EDX results, except Sn and Nd, O and Cl are also detected in the sample. The O and Cl comes from NdOCl. The atomic ratios of Sn to Nd are approximately 33:12, which is close to 3:1. That indicates the deposition of the Nd-Sn intermetallic compounds, NdSn<sub>3</sub>. The distribution of these elements in the product are shown in Figs. 7f–7i. From the EDX mapping results, the distribution of Sn and Nd is homogeneous and

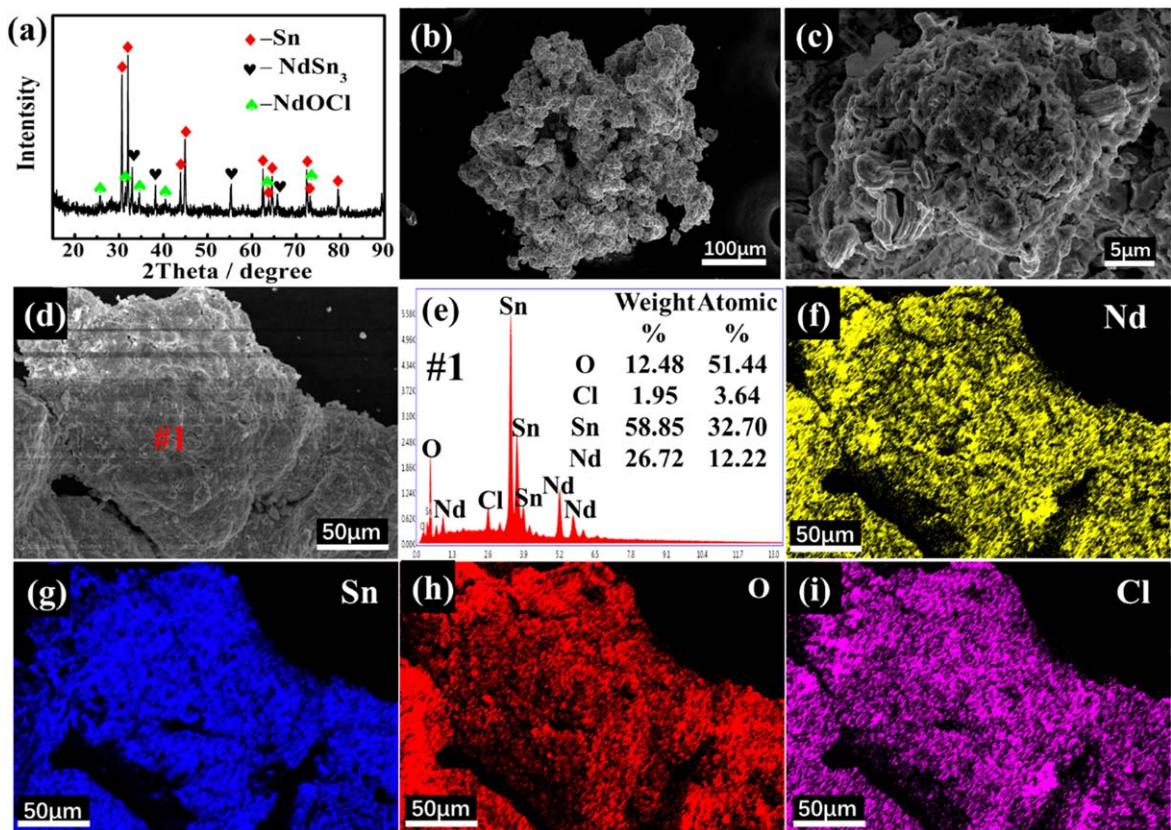


Figure 7. (a) XRD pattern of product, (b-d) SEM images and (e) EDS and corresponding element mapping of (f). Nd (g). Sn, (h). O, (i). Cl.

hard to distinguished from the EDS mapping image of surface deposition.

The solidified liquid Sn electrode is also detected by SEM-EDX. Figures 8a–8c shows the cross section of SEM image and the corresponding EDX result. It is clear to see that the Nd-contained inclusion is found in the solidified Sn electrode. The atomic ratios of Sn to Nd are approximately 9:24. It is much higher than the ratios in surface product. The formation of the high-Nd product in the solidified Sn electrode might be caused by the segregation during the solidification

process. From EDX mapping images in Figs. 8d–8f, the distribution of O accorded with the Nd, which might come from the oxidization of Nd alloy during the sanding and polishing process.

### Conclusions

In this work, the electrochemical behaviors of  $\text{Li}^+$  and  $\text{Nd}^{3+}$  on the liquid Sn electrode in the  $\text{LiCl-KCl-NdCl}_3$  melt was studied by various electrochemical technologies at 673 K.

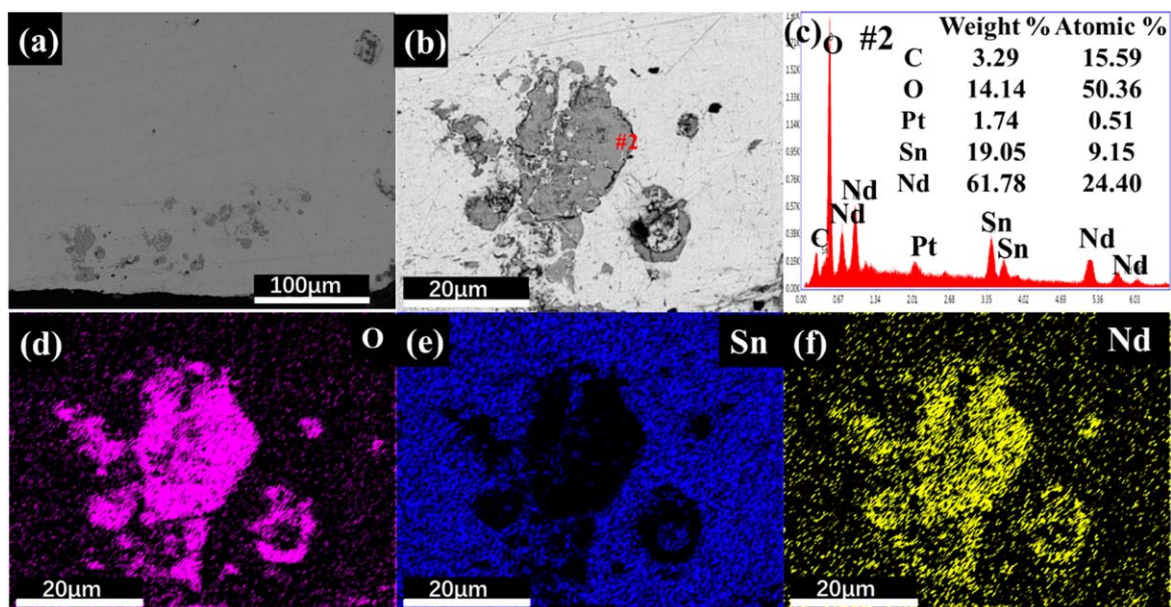


Figure 8. (a)–(c) SEM images and EDS result of the cross section of solidified liquid Sn electrode and corresponding element mapping of (d) O, (e) Sn, (f) Nd.

- (1)  $\text{Nd}^{3+}$  was reduced by two-step process in the W electrode and one-step process in the Sn electrode. The reduction potentials of  $\text{Nd}^{3+}$  on W and Sn electrodes at 673 K are  $-3.1$  and  $-2.5$  V vs  $\text{Cl}_2/\text{Cl}^-$ , respectively. The equilibrium potentials of  $\text{NdSn}_3$  and  $\text{Nd}_2\text{Sn}_5$  are  $-2.6$  and  $-2.9$  V, respectively. The equilibrium potential of  $\text{Li}_{[\text{Sn}]}$  at 673 K is  $-2.77$  V vs  $\text{Cl}_2/\text{Cl}^-$ .
- (2) Due to the reduction potential of  $\text{Li}_{[\text{Sn}]}$  stays between  $\text{NdSn}_3$  and  $\text{Nd}_2\text{Sn}_5$ , no  $\text{Li}_{[\text{Sn}]}$  would be reduced during the formation of  $\text{NdSn}_3$  at 673 K. During the formation of  $\text{Nd}_2\text{Sn}_5$  or other high Nd-contained Nd-Sn intermetallic compounds, it is inevitable to reduce Li in the Sn electrode.
- (3) After potentiostatic electrolysis at  $-2.74$  V, intermetallic compound  $\text{NdSn}_3$  existed in the precipitated phase. Besides, the rich Nd-contained inclusion was also found in the solidified Sn electrode.
- (4) To produce high Nd-contained Nd-Sn intermetallic compounds, the anodic ions ( $\text{M}^{n+}$ ) in the electrolyte should be carefully chosen. The M-Sn intermetallic compounds' formation potential should be negative than  $-3.6$  V vs  $\text{Cl}_2/\text{Cl}^-$ .

### Acknowledgments

This work was supported by Natural Science Foundation of China (No. 51574163).

### ORCID

Chenteng Sun  <https://orcid.org/0000-0003-2150-3726>

### References

1. Q. Wang, Y. Chen, S. Xiao, X. Zhang, Y. Tang, S. Wei, and Y. Zhao, *J. Rare Earths*, **28**, 790 (2010).
2. J. Wang, J. Fu, X. Dong, and Y. Yang, *Materials & Design (1980-2015)*, **36**, 432 (2012).

3. G. Hu, D. Zhang, F. Guo, L. Jiang, D. Yu, and F. Pan, *J. Rare Earths*, **32**, 52 (2014).
4. Y.-H. Hu, S.-B. Xue, H. Wang, H. Ye, Z.-X. Xiao, and L.-L. Gao, *J. Mater. Sci., Mater. Electron.*, **22**, 481 (2010).
5. J. Zhou, D. Huang, Y.-L. Fang, and F. Xue, *J. Alloys Compd.*, **480**, 903 (2009).
6. S.-Q. Jiao, H.-D. Jiao, W.-L. Song, M.-Y. Wang, and J.-G. Tu, *Int. J. Miner. Metall. Mater.*, **27**, 1588 (2020).
7. L.-X. Luo, Y.-L. Liu, N. Liu, L. Wang, L.-Y. Yuan, Z.-F. Chai, and W.-Q. Shi, *Electrochim. Acta*, **191**, 1026 (2016).
8. G. De Córdoba, A. Laplace, O. Conocar, J. Lacquement, and C. Caravaca, *Electrochim. Acta*, **54**, 280 (2008).
9. V. Smolenski, A. Novoselova, A. Osipenko, M. Kormilitsyn, and Y. Luk'yanova, *Electrochim. Acta*, **133**, 354 (2014).
10. K. Liu, Y.-L. Liu, Z.-F. Chai, and W.-Q. Shi, *J. Electrochem. Soc.*, **164**, D169 (2017).
11. T. Yin, Y. Liu, D. Yang, Y. Yan, G. Wang, Z. Chai, and W. Shi, *J. Electrochem. Soc.*, **167**, 122507 (2020).
12. S. Vandarkuzhali, M. Chandra, S. Ghosh, N. Samanta, S. Nedumaran, B. Prabhakara Reddy, and K. Nagarajan, *Electrochim. Acta*, **145**, 86 (2014).
13. C. Sun, Q. Xu, X. Zou, H. Cheng, and X. Lu, *Electrochem. Commun.*, **130**, 107111 (2021).
14. Y.-D. Yan, Y.-L. Xu, M.-L. Zhang, Y. Xue, W. Han, Y. Huang, Q. Chen, and Z.-J. Zhang, *J. Nucl. Mater.*, **433**, 152 (2013).
15. M. Li, Z. Sun, W. Han, Y. Sun, X. Yang, and W. Wang, *J. Electrochem. Soc.*, **167**, 022502 (2020).
16. H. Xu, M. Zhang, Y. Yan, D. Ji, P. Wang, M. Qiu, and L. Liu, *The Journal of Physical Chemistry C*, **122**, 3463 (2018).
17. S. Jiang, K. Liu, Y. Liu, T. Yin, Z. Chai, and W. Shi, *J. Nucl. Mater.*, **523**, 268 (2019).
18. J.-W. Pang, K. Liu, Y.-L. Liu, C.-M. Nie, L.-X. Luo, L.-Y. Yuan, Z.-F. Chai, and W.-Q. Shi, *J. Electrochem. Soc.*, **163**, D750 (2016).
19. M. Li, Q. Gu, W. Han, X. Zhang, Y. Sun, M. Zhang, and Y. Yan, *RSC Adv.*, **5**, 82471 (2015).
20. H. Jiao, J. Wang, L. Zhang, K. Zhang, and S. Jiao, *RSC Adv.*, **5**, 62235 (2015).
21. H. Jiao, S. Jiao, W.-L. Song, H. Chen, M. Wang, J. Tu, and D. Fang, *J. Electrochem. Soc.*, **166**, E401 (2019).
22. D. Henriques, V. Motalov, L. Bencze, S. Fürtauer, and T. Markus, *J. Alloys Compd.*, **585**, 299 (2014).
23. S. L. Wang, X. H. Su, S. S. Li, C. Y. Fu, Y. H. Guo, Y. X. Huang, D. H. Xiang, C. P. Wang, and X. J. Liu, *Calphad*, **60**, 214 (2018).
24. M. Ebner, F. Marone, M. Stampanoni, and V. Wood, *Science*, **342**, 716 (2013).